Nanoscale

Accepted Manuscript

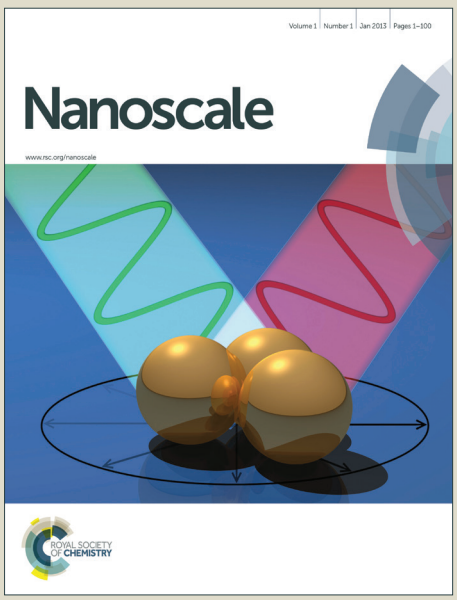

ROYAL SOCIETY OF CHEMISTRY

www.rsc.org/nanoscale

Cite this: DOI: 10.1039/c0xx00000x

www.rsc.org/xxxxxx

ARTICLE TYPE

Indirect Growth of Mesoporous Bi@C Core-shell Nanowires for Enhanced Lithium-Ion Storage

Rui Dai, Yuhang Wang, Peimei Da, Hao Wu, Ming Xu and Gengfeng Zheng*

Received (in XXX, XXX) Xth XXXXXXXXX 20XX, Accepted Xth XXXXXXXXX 20XX

DOI: 10.1039/b000000x

In this paper, we propose a facile synthetic strategy of uniform bismuth@carbon (Bi@C) core-shell nanowires, which are prepared via a controlled pyrolysis of Bi_2S_3@glucose-derived carbon-rich polysaccharide (GCP) nanowires under an inert atmosphere. The carbonization of GCP and the pyrolysis of Bi_2S_3 into Bi occur at 500 and 600 °C, respectively, which increase the specific surface area and the pore volume of the nanowires, thus allowing for accommodation of more lithium ions. Meanwhile, the carbon shell serves as a buffer layer to relieve large volume expansion/contraction during the electrochemical alloy formation, and can also efficiently reduce the aggregation of the nanowires. As a proof-of-concept, the Bi@C core-shell nanowire anodes manifest enhanced cycling stability (408 mA h g^{-1} after 100 cycles at a current density of 100 mA g^{-1}) and rate capacity (240 mA h g^{-1} at a current density of 1 A g^{-1}), much higher than pure bismuth microparticles and corresponding Bi_2S_3@C nanowires.

Introduction

The continuous demand of energy storage has been driving the development of new lithium-ion battery electrodes with superior energy density, fast charge/discharge rate, and durable cycling performance.[1] Metals of group IV (Ge, Sn) and group V (Sb, Bi) and their corresponding alloys, due to their ability to react reversibly with large amounts of lithium per formula unit, have attracted much attention as LIB anode materials.[2-5] For instance, bismuth (Bi) has been reported to react with lithium to obtain a theoretical gravimetric capacity of 385 mA h g^{-1} (as Li_3Bi),[6] comparable to that of the commercial graphite anode. In addition, attributed to the relatively high density of Bi, its volumetric capacity can even reach as high as ca. 3800 mA h cm^{-3},[7] thus highlighting its potential as an advantageous anode material in the practical applications of battery systems for electronic mobile devices. Nonetheless, anodes made of pure Bi metal typically result in poor electrochemical performance,[6] as the substantial volume increase upon Li^+ intercalation inevitably leads to a dramatic volume increase (~215%) and subsequent electrode pulverization.[8] Reducing the size of Bi materials to nanoscale regime may partly alleviate the volume-change problem. For instance, Bi nanowires and nanospheres have been reported via electrodeposition[9] and thermolysis methods.[10] Nonetheless, the aggregation of those nano-sized materials during electrochemical processes can also hinder the cycling performance of anodes.[11,12] On the other hand, carbon coating and pore formation are two potential solutions for reducing electrode aggregation or volume change. However, carbon coating on existing nanostructures typically requires high processing temperatures, while due to the low melting point of Bi (~ 270 °C),[13] the controlled coating of a thin carbon layer on Bi nanostructures is extremely challenging.

Bismuth sulfide (Bi_2S_3) is one of the most common bismuth compounds and can be controllably synthesized as a large variety of 1-dimensional (1D) morphologies using solvothermal and hydrothermal approaches.[14] Although it has a high theoretical gravimetric capacity of 625 mA h g^{-1},[15] its low electrical conductivity often requires incorporating conductive materials such as carbon for potential application in LIBs.[15-17] Furthermore, it has been reported that the regeneration of Bi_2S_3 may not be reversible during the Li^+ insertion/extraction process, during which metal Bi is the main active material for Li-storage after several cycles.[15,18] Bi_2S_3 is a stable compound but can be decomposed into Bi at relative high temperatures (>600 °C, depending on the calcination condition).[19] It is thus advantageous to use the relative stable and easily obtained Bi_2S_3 nanostructures as a precursor to synthesize the targeted Bi@C core-shell nanowires through a thermal conversion.

Herein, we developed a facile approach for synthesis of mesoporous, carbon-coated Bi (Bi@C core-shell) nanowires (NWs), via a hydrothermal growth of Bi_2S_3 NWs followed by thermal decomposition. As schematically shown in Figure 1, single-crystalline Bi_2S_3 NWs are first synthesized by a hydrothermal method, using bismuth nitrate and thioacetamide as precursors (Experimental section). Afterwards, a layer of glucose-derived carbon-rich polysaccharide (GCP) is coated onto the surface of Bi_2S_3 NWs under hydrothermal conditions, in which glucose undergoes dehydration, polymerization, aromatization and carbonization process.[20, 21] Subsequent thermal calcinations of the Bi_2S_3@GCP NWs under an inert atmosphere can carbonize the outer GCP shell into carbon, and at the same time decompose the inner Bi_2S_3 core into Bi metal NWs. Due to

the confinement of carbon shell, the resulting Bi cores still maintain the NW structure. Furthermore, the in-situ pyrolysis of Bi_2S_3 leads to the formation of mesopores inside the Bi@C core-shell NW structure, resulting in an increase of surface area and pore volume, which can also alleviate the impact of volume expansion on the electrode cycle life. As a proof-of-concept, LIB anodes made of the obtained Bi@C core-shell NWs show much enhanced reversible capacity and excellent cycling performance (408 mA h g^{-1} after 100 cycles at a current density of 100 mA g^{-1}), as well as good charge-rate capabilities (240 mA h g^{-1} at a current density of 1 A g^{-1}), suggesting its potential as a promising LIB anode material.

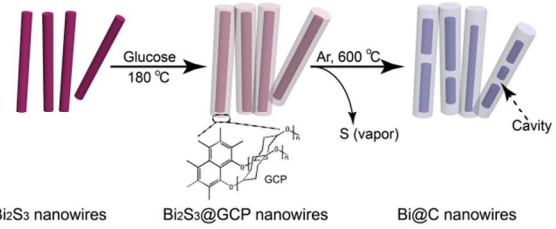

Fig. 1 Synthetic scheme of mesoporous Bi@C nanowires.

Experimental

Chemicals

$Bi(NO_3)_3{\cdot}5H_2O$, thioacetamide (TAA), concentrated HCl (36.0~38.0 wt%) and glucose were of analytical grade and purchased from Shanghai Chemical Corp. Bismuth powder (Bi microparticles, 5N) was also purchased from Shanghai Chemical Corp. All chemicals were used as received without further purification. De-ionized (DI) water was used for all experiments.

Synthesis

The Bi@C core-shell NWs were prepared via three main steps, as shown in Figure 1. Firstly, Bi_2S_3 NWs were prepared via a hydrothermal method, in which 0.75 mmol $Bi(NO_3)_3{\cdot}5H_2O$ and 2.25 mmol TAA were dissolved in a solution containing 1.5 mL of HCl and 15 mL of H_2O. The mixture was stirred for 5 min before transferred into a 25-mL Teflon-lined autoclave with stainless steel shell and heated in an air-flow electric oven at 120 °C for 12 h. The black product (Bi_2S_3 NWs) was collected by centrifugation, washed with H_2O then ethanol, and dried at 60 °C. Afterwards, carbon-rich polysaccharide was coated onto Bi_2S_3 NWs by pyrolysis of glucose under hydrothermal conditions, forming Bi_2S_3@GCP NWs. In a typical synthesis, 0.1 g of as-prepared Bi_2S_3 NWs was dispersed in 20 mL, 0.5 M aqueous glucose solution by stirring and ultrasonication. The suspension was transferred to a 25-mL Teflon-lined stainless steel autoclave and heated at 180 °C for 3 h. The dark brown product was harvested by centrifugation and washed with DI water and ethanol repeatedly. After drying at 60 °C in oven, the Bi_2S_3@GCP NWs was calcined at 600 °C for 4 h under an Ar flow (100 sccm), during which the GCP shell was carbonized and the inner Bi_2S_3 was decomposed, forming mesoporous Bi@C core-shell NWs. The gaseous sulfur produced from the decomposition of Bi_2S_3 was condensed at the low temperature zone of the quartz tube along the direction of the carrier gas flow.

For a comparison, Bi_2S_3@C core-shell NWs were prepared followed almost the same strategy, except that the calcination temperature was set at 500 °C.

Physicochemical characterization

The Bi@C NWs were characterized by field-emission scanning electron microscopy (SEM, Hitachi S-4800, Japan) and transmission electron microscopy (TEM, JEM-2100F, Japan). X-ray diffraction data were collected on an X-ray diffractometer (XRD, Bruker SMART APEX (II)-CCD, Germany). N_2 sorption isotherms were measured at 77 K by using a Micro-metrics ASAP 2420 system, with surface area and pore size obtained by using Brunauer-Emmett-Teller (BET) and Barrett-Joyner-Halenda (BJH) methods. Thermogravimetric analysis was carried out by a thermo gravimetric analyzer (Perkin-Elmer TGA7, USA). Element contents were analyzed by an inductive coupled plasma-mass (ICP) spectrometer (ICP-AES, Hitachi P-4010, Japan).

Electrochemistry characterization

For electrochemical evaluation of the obtained samples, a slurry consisting of 80% active powder material, 10% acetylene black as a conductor, and 10% polyvinylidene fluoride (PVDF) as a binder was dispersed in N-methyl pyrrolidinone (NMP) in an ambient environment. The slurry was then coated onto a copper foil current collector, baked at 80 °C in vacuum for over 10 h. The loading density of active material on current collector is > 1 mg cm^{-2}. The 2016 coin-type cells were assembled in an Ar-filled glove box, with pure lithium foils used as the counter electrodes. $LiPF_6$ (1M) in ethylene carbonate (EC)/ diethyl carbonate (DEC)/ dimethyl carbonate (DMC) (1:1:1 w/ w/ w) was used as the electrolyte. The cycling performance of all cells was tested using a multi-channeled battery tester (Neware Co., China). The cyclic voltammetry and A.C. impedance were measured on a CHI660D electrochemical workstation (CHI Inc., USA).

Results and Discussion

Composition and structural characterization

After the hydrothermal synthesis of Bi_2S_3, SEM images show that the obtained samples have a NW structure, with an average diameter of ca. 50 nm (**Fig. 2a**). After coated with glucose-derived carbon-rich polysaccharide shells, the surface of the NWs becomes much smoother with no sharp edges, indicating a uniform coating of GCP shell outside the Bi_2S_3 NWs (**Fig. S1**). After carbonized at 500 and 600 °C, the Bi_2S_3@C and Bi@C core-shell NWs are obtained, respectively (**Fig. 2b, c**), with almost no significant change of the external morphology observed. The composition and crystal structures of these compounds were first analyzed by XRD. For the pristine compound (**Fig. 2d**, black curve), several distinct diffraction peaks are displayed at 15.8, 17.6, 22.4, 24.9, 28.6, 31.8, 35.6, 39.9, 46.7 degrees, corresponding to the (020), (120), (220), (130), (211), (221), (240), (141), (501) diffractions of a Bi_2S_3 crystal structure (JCPDS No. 17- 0320). After the hydrothermal carbon coating and subsequent 500 °C carbonization process, no phase change is observed for the product (**Fig. 2d**, blue curve), indicating the Bi_2S_3 structure is still maintained. When the carbonization temperature is increased to 600 °C, all diffraction peaks of the product (**Fig. 1d**, red curve) are in good agreement

with hexagonal bismuth (JCPDS No.44- 1246), confirming that the Bi_2S_3 core is converted into metal bismuth by 600 °C pyrolysis.

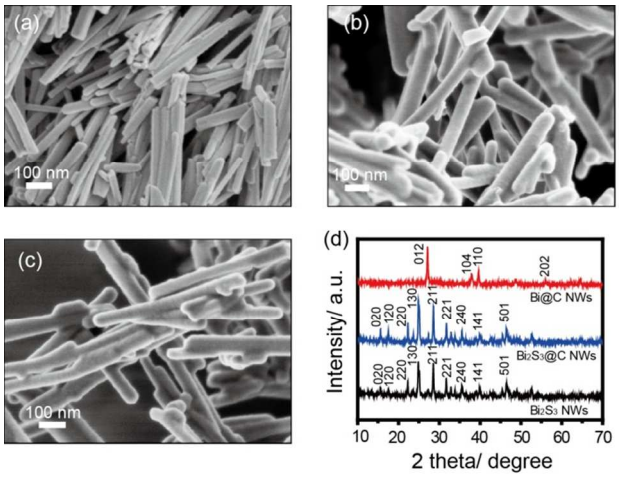

Fig. 2 SEM images of (a) Bi_2S_3 NWs, (b) Bi_2S_3@C core-shell NWs and (c) Bi@C core-shell NWs; (d) XRD curves of Bi_2S_3 NWs (bottom), Bi_2S_3@C core-shell NWs (middle), and Bi@C core-shell NWs (top).

The difference between Bi_2S_3@C and Bi@C core-shell NWs are further exhibited by TEM. Each individual Bi_2S_3 NW is encapsulated in a carbon shell with diameter of no more than 20 nm, and almost no agglomeration of Bi_2S_3 NWs is observed (**Fig. 3a**). An amorphous carbon shell is uniformly coated on the NW surface. High-resolution TEM (HRTEM) images and the selected area electron diffraction (SAED) pattern exhibit that the obtained Bi_2S_3 NW core is a single-crystalline orthorhombic structure,[22,23] with the lattice fringes spacing of 0.36 nm (**Fig. 3b** and **inset**), well corresponding to the lattice constant of the (130) plane, which is also consistent with the XRD results. For the Bi@C core-shell NWs, cavities are observed inside the NW cores (**Fig. 3c, Fig. S2**), which are ascribed to the pore formation during the pyrolysis step. The HRTEM images of the Bi@C core-shell NWs reveal the crystalline Bi core and an amorphous carbon shell (**Fig. 3d**). As the nanostructured bismuth is not stable under the TEM beam irradiation, the SAED pattern shows translation between regular single-crystalline diffraction patterns and irregular polycrystalline diffraction rings (**Fig. 3d inset**), which finally exhibit a distinct set of lattice fringes attributed to the diffraction of the (012) and (104) planes of metal Bi, in good accord with the XRD results.

To confirm the composition of the Bi@C core-shell NWs, energy-dispersive X-ray (EDX) spectroscopy was carried out (**Fig. S3a**). The peaks of C and Bi are clearly identified, and the relatively strong Cu peaks are originated from Cu mesh supporting the sample. The compositions of the Bi@C core-shell NWs are analyzed to be 23 wt% of carbon and 77 wt% of Bi, which are further confirmed by the ICP test. Furthermore, the scanning TEM (STEM) images and the corresponding elemental mapping of the Bi@C NWs clearly demonstrate the inner Bi core and outer carbon shell (**Fig. S3b-d**), thus further demonstrating a uniform distribution of these two elements in the nanocomposites.

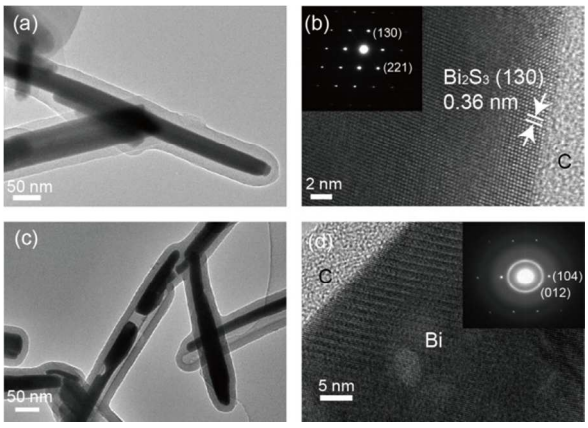

Fig. 3 TEM and HRTEM images of (a, b) Bi_2S_3@C core-shell NWs and (c, d) Bi@C core-shell NWs. Insets in b, d are the SAED patterns.

The conversion process from the Bi_2S_3@GCP core-shell NWs into the Bi@C core-shell NWs is investigated by the thermogravimetric (TG) analysis under N_2. Four valleys in the differential TG (DTG) curve are clearly observed (**Fig. S4**, black line). The first and second weight losses take place under 200 °C, which are ascribed to the loss of free water (absorption water) and the loss of crystalliferous water during heating process, respectively. The third mass loss between 200 and 400 °C corresponds to the carbonization process of the GCP shell, resulting in the formation of carbon shell of the nanocomposites. The fourth mass loss taking place between 500 and 600 °C can be attributed to the reduction of Bi_2S_3 to Bi. Although the decomposition temperature of bulk Bi_2S_3 is higher than 600 °C,[19] an enhanced reactivity is expected when the crystal sizes are reduced to nanoscale, which has already been shown by the thermodynamic behaviours of other micro/nanosystems.[24] Thus, when the Bi_2S_3@GCP core-shell NWs are sequentially heated to 500 and 600 °C under an inert atmosphere, the following two pyrolysis steps occur:

Bi_2S_3@GCP → Bi_2S_3@C → Bi@C + S (vapor)

Nitrogen sorption isotherm measurements were carried out to measure the specific surface area and pore volume change of the Bi_2S_3@GCP core-shell NWs caused by the pyrolysis at 500 and 600 °C, respectively. Both isotherms show a type IV sorption shape with a hysteresis loop (**Fig. S5**), indicating the formation of a mesoporous structure.[25] The BET specific surface area and the pore volume calculated from the N_2 sorption measurements are 169.69 $m^2\ g^{-1}$ and 0.028 $cm^3\ g^{-1}$ after 500 °C calcination, and increased to 194.23 $m^2\ g^{-1}$ and 0.038 $cm^3\ g^{-1}$ after 600 °C calcination. These increases in both the specific surface area and the pore volume observed between the 500 and 600 °C calcinations are ascribed to the formation of new mesopores by pyrolysis of Bi_2S_3 at 600 °C, consistent with our TEM and TG results.

The electrochemical properties of the obtained Bi@C core-shell NWs are then investigated as rechargeable LIB anodes (Experimental section). The cycle voltammetry (CV) curves of the Bi@C core-shell NW anodes are first displayed to illustrate the electrochemical reactions (**Fig. 4a**). An irreversible broad peak between 1.2–2 V in the first cathodic scan can be attributed to the formation of a solid electrolyte interphase (SEI) layer on

the carbon surface, as a result of the reductive decomposition of the electrolyte, which gives rise to the large irreversible capacity loss during the first cycle.[26-29] The peaks between 0.5–1 V during charging and the ones between 0.8–1.2 V during discharging are ascribed to the phase transitions between Bi, LiBi and Li_3Bi, respectively, indicating good reversibility in electrochemical reaction pathways and consistent with the literatures.[7,8,30]

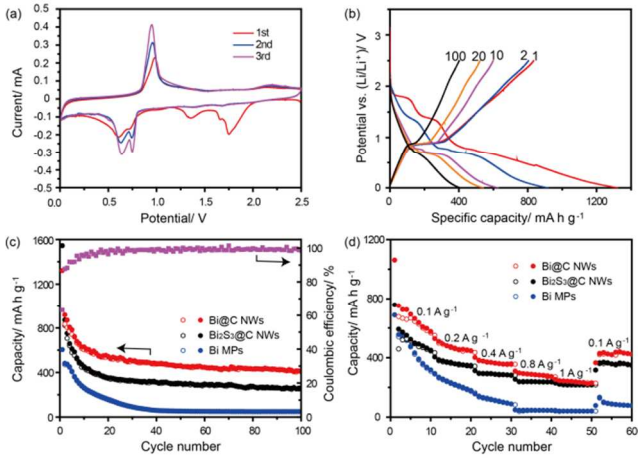

Fig. 4 (a) Cyclic voltammograms of the Bi@C core-shell NWs (scan rate = 0.1 mV s^{-1}); (b) Charge/discharge curves of the Bi@C core-shell NWs at a current density of 100 mA g^{-1}; (c) Cycling performance of commercial Bi microparticles, Bi_2S_3@C core-shell NWs and Bi@C core-shell NWs, at a current density of 100 mA g^{-1}; (d) Cycling performance of commercial Bi microparticles, Bi_2S_3@C core-shell NWs and Bi@C core-shell NWs at different current densities from 0.1 to 1 A g^{-1}.

The discharge/charge potential profiles of the Bi@C core-shell NW anodes were further measured, with several representative cycles of the 1st, 2nd, 10th, 20th and 100th cycles displayed (**Fig. 4b**). The first discharge and charge capacities are measured as 1322 and 834.1 mA h g^{-1}, respectively, with an initial Coulombic efficiency of 63.1%. The much higher initial capacity of the Bi@C core-shell NWs can be attributed to the thin carbon layer and many cavities encapsulated in the Bi cores, providing relatively large specific surface area and pore volume. The specific capacities decrease rapidly during the first 10 cycles, and become much more stable during the 10–100 cycles. The quick drop of the capacities in the initial cycles is associated to the SEI formation, while as the cycle number increases, the relatively large specific surface area and pore volume play a positive role in compensation of the volume expansion, thus exhibiting greatly improved capacity retention and stability. Similar phenomenon has also been reported on other carbon-based nanocomposites.[31-33]

The cycling stability of the Bi@C core-shell NW anodes was measured between 2.5 and 0 V, and compared with anodes made from commercial Bi microparticles (**Fig. S6**) and the Bi_2S_3@C core-shell NWs. The capacity of the Bi microparticles and the Bi_2S_3@C core-shell NWs drop much more rapidly than that of the Bi@C core-shell NWs (**Fig. 3c**). An excellent capacity retention of the Bi@C core-shell NWs is obtained, with a reversible capacity of 408 mA h g^{-1} over 100 cycles at a current density of 100 mA g^{-1}. This value is slighly higher than the theoretical gravimetric capacity of Bi, which can be attributed to the thin and porous surface carbon layer that allows for higher absorption of Li-ions,[34] or the reversible conversion of some SEI components formed on the surface of Bi@C core-shell NWs with a large specific area and many vacancies.[35] The rate performances of these three anodes were further investigated, with varied current densities from 0.1 to 1 A g^{-1} (**Fig. 4d**). The capacity of the Bi microparticles drops quickly to almost negligible, suggesting that most of the inner materials are not lithiated at higher rates. In contrast, the Bi@C core-shell NWs exhibit the highest rate performance among these three electrodes, suggesting the contribution from both the porous Bi NW core and the carbon layer protection.

The enhanced capacity of the Bi@C core-shell NWs can be attributed to the synthesis approach and resulting structures. The carbon shells prevent the aggregation, and the substantial increase of surface area and pore volume derived from pyrolysis can contribute to enhanced surface electrochemical reactions and effectively accommodate volume expansion. [36] In addition, although Bi_2S_3 has a higher theoretical gravimetric capacity (625 mA h g^{-1}) than Bi (386 mA h g^{-1}), the nano-sized Bi cores substantially shorten the diffusion distance and increase the transport efficiency of Li^+.[37] This effect is demonstrated by the electrochemical impedance spectroscopy (EIS) measurement.[38] The charge transfer impedances of the Bi@C core-shell NWs, Bi_2S_3@C core-shell NWs and Bi microparticles were measured before (**Fig. 5a**) and after (**Fig. 5b**) battery cycling. All the Nyquist plots were obtained at amplitude of 10 mV versus the same potential of 0.8 V with a frequency range of 0.01 Hz to 100 kHz. The charge transfer process at the electrode interface is deduced from the depressed semicircle of the Nyquist plot in the high frequency region. The diameter of the semicircle for the Bi@C core-shell NWs is the smallest of the three samples, indicating the lowest charge transfer impedance. By using an equivalent circuit model (**Fig. S7**), the charge transfer impedances of the Bi@C core-shell NWs are calculated to be 11.05 and 17.28 Ω before and after cycling, respectively. These small and similar impedances before and after cycling partly illustrate the hypothesis of the origin for the electrochemical performance enhancement of the Bi@C core-shell NWs. Moreover, the SEM images of the three electrodes collected after 10 charge/discharge cycles show that the Bi@C core-shell NWs have the best morphology retention (**Fig. S8**), which is attributed to the coated carbon shell and the porous core structures.[39]

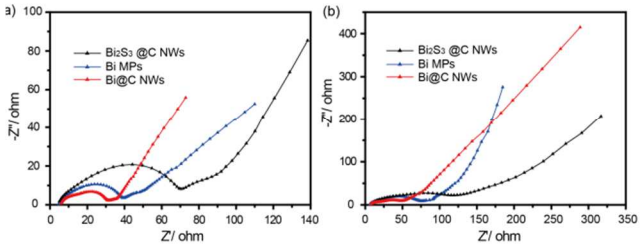

Fig. 5 Electrochemical impedance spectra of electrodes made of commercial Bi microparticles, Bi_2S_3@C core-shell NWs and Bi@C core-shell NWs, (a) before and (b) after battery cycling. Here Z' and Z'' are represented as resistance and capacitance.

Conclusions

In summary, a controlled pyrolysis strategy has been developed to prepare mesoporous Bi@C core-shell NWs, by calcinations of a hybrid Bi_2S_3@GCP NWs in an inert atmosphere. The in-situ decomposition of Bi_2S_3@GCP NWs can well retain the 1D nanostructures, while at the same time produce mesopores in the Bi NW cores. Together with the amorphous carbon shell, these formed mesopores can increase the Li^+ storage as well as the structure flexibility, and alleviate the pressure of volume expansion during Li^+ intercalation/de-intercalation. As a proof-of-concept, the Bi@C core-shell NWs have shown much enhanced reversible Li^+ storage capacity and cycling performance. Our approach has not only provided an example of the Bi-based nanostructures for LIB anodes, but also suggested new synthetic designs of other carbon-coated metals or alloys for enhanced energy storage.

Acknowledgements

We thank the following funding agencies for supporting this work: the National Key Basic Research Program of China (2013CB934104), the Natural Science Foundation of China (21322311, 21473038, 21071033), the Science and Technology Commission of Shanghai Municipality (14JC1490500), the Doctoral Fund of Ministry of Education of China, the Program for Professor of Special Appointment (Eastern Scholar) at Shanghai Institutions of Higher Learning, and the Deanship of Scientific Research of King Saud University (IHCRG#14-102).

Notes

Laboratory of Advanced Materials, Department of Chemistry, Fudan University, Shanghai 200433, People's Republic of China; E-mail: gfzheng@fudan.edu.cn

References

1. J. M. Tarascon and M. Armand, *Nature,* 2001, **414,** 359-367.
2. C. K. Chan, X. F. Zhang and Y. Cui, *Nano Lett. ,* **2008,** 8, 307-309.
3. J. X. Zhu, T. Sun, J. S. Chen, W. H. Shi, X. J. Zhang, X. W. Lou, S. Mhaisalkar, H. H. Hng, F. Boey, J. Ma and Q. Y. Yan, *Chem. Mater. ,* 2010, **22,** 5333-5339.
4. H. Lee and J. Cho, *Nano Lett. ,* 2007, **7,** 2638-2641.
5. C. J. Liu, F. H. Xue, H. Huang, X. H. Yu, C. J. Xie, M. S. Shi, G. Z. Cao, Y. G. Jung and X. L. Dong, *Electrochim. Acta,* 2014, **129,** 93-99.
6. A. Finke, P. Poizot, C. Guery, L. Dupont, P. L. Taberna, P. Simon and J. M. Tarascon, *Electrochem. Solid State Lett. ,* 2008, **11,** E5-E9.
7. C. M. Park, S. Yoon, S. I. Lee and H. J. Sohn, *J. Power Sources,* 2009, **186,** 206-210.
8. O. Crosnier, T. Brousse, X. Devaux, P. Fragnaud and D. Schleich, *J. Power Sources,* 2001, **94,** 169-174.
9. L. Li, Y. W. Yang, X. S. Fang, M. G. Kong, G. H. Li and L. D. Zhang, *Solid state commun. ,* 2007, **141,** 492-496.
10. Y. Wang, J. Chen, L. Chen, Y. B. Chen and L. M. Wu, *Cryst. Growth Des. ,* 2010, **10,** 1578-1584.
11. L. W. Ji and X. W. Zhang, *Electrochem. Commun. ,* 2009, **11,** 1146-1149.
12. J. X. Zhu, T. Zhu, X. Z. Zhou, Y. Y. Zhang, X. W. Lou, X. D. Chen, H. Zhang, H. H. Hng and Q. Y. Yan, *Nanoscale,* 2011, **3,** 1084-1089.
13. Y. D. Li, J. W. Wang, Z. X. Deng, Y. Y. Wu, X. M. Sun, D. P. Yu and P. D. Yang, *J. Am. Chem. Soc. ,* 2001, **123,** 9904-9905.
14. J. M. Ma, J. Q. Yang, L. F. Jiao, T. H. Wang, J. B. Lian, X. C. Duan and W. J. Zheng, *Dalton Trans. ,* 2011, **40,** 10100-10108.
15. H. Jung, C. M. Park and H. J. Sohn, *Electrochim. Acta,* 2011, **56,** 2135-2139.
16. Z. A. Zhang, C. K. Zhou, H. Lu, M. Jia, Y. Q. Lai and J. Li, *Mater. Lett. ,* 2013, **91,** 100-102.
17. Y. Zhao, D. L. Gao, J. F. Ni, L. J. Gao, J. Yang and Y. Li, *Nano Res. ,* 2014, **7,** 765-773.
18. Z. A. Zhang, C. K. Zhou, L. Huang, X. W. Wang, Y. H. Qu, Y. Q. Lai and J. Li, *Electrochim. Acta,* 2013, **114,** 88-94.
19. R. Padilla, R. Villa and M. C. Ruiz, *2nd International Symposium on High-Temperature Metallurgical Processing,* 2011, 221-228.
20. X. M. Sun and Y. D. Li, *Angew. Chem. Int. Ed. ,* 2004, **43,** 597-601.
21. T. Zhu, J. S. Chen and X. W. Lou, *J. Phys. Chem. C,* 2011, **115,** 9814-9820.
22. H. Zhang, Y. J. Ji, X. Y. Ma, J. Xu and D. R. Yang, *Nanotech.,* 2003, **14,** 974-977.
23. G. J. Xiao, Q. F. Dong, Y. N. Wang, Y. M. Sui, J. J. Ning, Z. Y. Liu, W. J. Tian, B. B. Liu, G. T. Zou and B. Zou, *RSC Adv. ,* 2012, **2,** 234-240.
24. R. Liu, T. L. Zhang, L. Yang and Z. N. Zhou, *Thermochim. Acta,* 2014, **583,** 78-85.
25. K. S. W. Sing, D. H. Everett, R. A. W. Haul, L. Moscou, R. A. Pierotti, J. Rouquerol and T. Siemieniewska, *Pure Appl. Chem. ,* 1985, **57,** 603-619.
26. X. Zhang, H. H. Liu, S. Petnikota, S. Ramakrishna and H. J. Fan, *J. Mater. Chem. A,* 2014, **2,** 10835-10841.
27. X. H. Cao, Y. M. Shi, W. H. Shi, X. H. Rui, Q. Y. Yan, J. Kong and H. Zhang, *Small,* 2013, **9,** 3433-3438.
28. L. F. Cui, J. Shen, F. Y. Cheng, Z. L. Tao and J. Chen, *J. Power Sources,* 2011, **196,** 2195-2201.
29. M. Zhang, D. N. Lei, X. Z. Yu, L. B. Chen, Q. H. Li, Y. G. Wang, T. H. Wang and G. Z. Cao, *J. Mater. Chem. ,* 2012, **22,** 23091-23097.
30. X. M. Wang, T. Nishina and I. Uchida, *J. Power Sources,* 2002, **104,** 90-96.
31. D. J. Xue, S. Xin, Y. Yan, K. C. Jiang, Y. X. Yin, Y. G. Guo and L. J. Wan, *J. Am. Chem. Soc. ,* 2012, **134,** 2512-2515.
32. W. M. Zhang, J. S. Hu, Y. G. Guo, S. F. Zheng, L. S. Zhong, W. G. Song and L. J. Wan, *Adv. Mater. ,* 2008, **20,** 1160-1165.
33. W. H. Li, Z. Z. Yang, J. X. Cheng, X. W. Zhong, L. Gu and Y. Yu, *Nanoscale,* 2014, **6,** 4532-4537.
34. B. Xu, L. Shi, X. W. Guo, L. Peng, Z. X. Wang, S. Chen, G. P. Cao, F. Wu and Y. S. Yang, *Electrochimica Acta*, 2011, **56,** 6464-6468.
35. L. W. Su, Y. R. Zhong and Z. Zhou, *J. Mater. Chem. A,* 2013, **1,** 15158-15166.
36. Y. L. Zhao, L. Xu, L. Q. Mai, C. H Han, Q. Y. An, X. Xu, X. Liu and Q. J. Zhang, *PNAS,* 2012, **109,** 19569-19574.
37. Y. X. Tang, Y. Y. Zhang, J. Y. Deng, J. Q. Wei, H. L. Tam, B. K. Chandran , Z. L. Dong , Z. Chen and X. D. Chen, *Adv. Mater.* 2014, 26, doi:10.1002/adma.201402000.
38. Y. X. Tang, Y. Y. Zhang, J. Y. Deng, D. P. Qi, W. R. Leow, J. Q. Wei, S. Y. Yin, Z. L. Dong, Z. Chen and X. D. Chen, *Angew. Chem. Int. Ed.* 2014, **53,** 1-6.
39. Y. Z. Luo , X. Xu , Y. X. Zhang , Y. Q Pi , Y. L Zhao , X. C Tian , Q. Y. An , Q. L. Wei and L. Q. Mai, *Adv. Energy Mater.,* DOI: 10.1002/aenm.201400107.